A NOVEL AUTOENCODER-BASED DIAGNOSTIC SYSTEM FOR EARLY ASSESSMENT OF LUNG CANCER

Ahmed Shaffie[1,2]*, Ahmed Soliman*[1]*, Mohammed Ghazal*[3,1]*,Fatma Taher*[4]*, Neal Dunlap*[5]*,*
Brian Wang[5]*,Victor van Berkel*[6]*, Georgy Gimel'farb*[7]*, Adel Elmaghraby*[2] *and Ayman El-Baz*[1*]

[1]BioImaging Laboratory, Bioengineering Department, University of Louisville, Louisville, KY, USA.

[2]Computer Engineering and Computer Science Department, University of Louisville, Louisville, KY, USA.

[3]Department of Electrical and Computer Engineering, Abu Dhabi University, Abu Dhabi, UAE

[4]College of Technological Innovation, Zayed University, Dubai, UAE

[5]Department of Radiation Oncology, University of Louisville, Louisville, KY, USA.

[6]Department of Cardiovascular and Thoracic Surgery, University of Louisville, Louisville, KY, USA

[7]Department of Computer Science, University of Auckland, Auckland, New Zealand.

ABSTRACT

A novel framework for the classification of lung nodules using computed tomography (CT) scans is proposed in this paper. To get an accurate diagnosis of the detected lung nodules, the proposed framework integrates the following two groups of features: *(i)* appearance features that is modeled using higher-order Markov Gibbs random field (MGRF)-model that has the ability to describe the spatial inhomogeneities inside the lung nodule; and *(ii)* geometric features that describe the shape geometry of the lung nodules. The novelty of this paper is to accurately model the appearance of the detected lung nodules using a new developed 7^{th}-order MGRF model that has the ability to model the existing spatial inhomogeneities for both small and large detected lung nodules, in addition to the integration with the extracted geometric features. Finally, a deep autoencoder (AE) classifier is fed by the above two feature groups to distinguish between the malignant and benign nodules. To evaluate the proposed framework, we used the publicly available data from the Lung Image Database Consortium (LIDC). We used a total of 727 nodules that were collected from 467 patients. The proposed system demonstrates the promise to be a valuable tool for the detection of lung cancer evidenced by achieving a nodule classification accuracy of 92.20%.

***Index Terms*—** Computed Tomography, Higher-order MGRF, Computer Aided Diagnosis

1. INTRODUCTION

Lung cancer is the second most common cancer in men and women all over the world. It comes after prostate cancer in men and after breast cancer in women [1]. The number of patients suffering from lung cancer has recently increased significantly all over the world, which increases the motivation in developing an accurate and fast diagnostic tools to detect lung cancer earlier in order to increase the patients' survival rate. Histological examination through biopsies is considered the gold standard for the final diagnosis of pulmonary nodules as malignant or benign. Even though resection of pulmonary nodules is the ideal and most reliable way for diagnosis. There is a crucial need for developing a non-invasive diagnostic tools to eliminate the risks associated with the surgical procedure.

*Corresponding author, e-mail: aselba01@louisville.edu.

In general, there are several imaging modalities used to diagnose the pulmonary nodules, like chest radiography (X-Ray), magnetic resonance imaging (MRI), positron emission tomography (PET) scan, and computed tomography (CT) scans. Some researchers prefer to use MRI to avoid exposing patient to ionizing radiation which has a very bad effect and gives the potential to increase lifetime cancer risk [2]. Diffusion Weighted MRI (DW MRI) has been reported to be used for lung cancer diagnosis, as it could be used to qualitatively checking the high $b-$value images and apparent diffusion coefficient (ADC) maps in addition to quantitatively generating the mean and median tumor ADCs [3]. However, CT and PET scans are the most widely used modalities for diagnosis and staging of lung cancer. A CT scan is more likely to show lung tumors than other modalities because of its high resolution and clear contrast compared to other modalities. We will focus and utilize the CT scans in our study as it is considered a routine procedure for patients who have lung cancer in addition to the high resolution pulmonary anatomical details.

Recently, a lot of researchers have tried to develop computer aided diagnostic (CADx) systems to classify the detected lung nodules to earlier detect lung cancer. Sun et al [4] studied the feasibility of using deep learning algorithms for benign/malignant classification on the Lung Image Database Consortium (LIDC) dataset. They designed and implemented three deep learning algorithms named Deep Belief Networks (DBNs), Convolutional Neural Network (CNN) and Stacked Denoising Autoencoder (SDAE). They compared the performance of deep learning algorithms with traditional CADx systems by designing a scheme with 28 image features and SVM. Shen et al [5] focused on modeling raw nodule patches without any prior definition of nodule morphology. They proposed a hierarchical learning framework based on Multi-scale Convolutional Neural Networks (MCNN), to capture nodule heterogeneity by extracting discriminative features from alternatingly stacked layers. Their framework used multi-scale nodule patches to learn a set of known features simultaneously by concatenating response neuron activations gotten at the last layer from each input scale. Another study by Nishio et al [6]performed contrast-enhanced CT in 46 CT examinations. Their method was based on novel patch-based feature extraction using principal component analysis, pooling operations and image convolution. They compared their method to three other systems for the extraction of nodule features: histogram of CT density, three-dimensional random local binary pattern and local

978-1-4799-7061-2/18/$31.00©2018 IEEE ICIP 2018

binary pattern on three orthogonal planes. They analyzed the probabilistic outputs of the systems and surrogate ground truth using receiver operating characteristic (ROC) curve and AUC. A SVM-based CAD system had Dhara et al [7] focused on the classification of nodules using SVM. Nodules were segmented using a semi-automated technique, which needed only a seed point from the user. They computed shape-based, margin-based, and texture-based features to represent the nodules. They determined a set of relevant features as a second step for an efficient representation of nodules in the feature space. Song et al [8] developed three types of deep neural networks (e.g., CNN, DNN, and SAE) for lung nodule calcification. They used those networks on the CT image classification task with some modification for the lung nodules. Shewaye et al [9] proposed an automated system to diagnose lung nodules in CT images. Experimental results were illustrated using a combination of histogram and geometric lung nodule image features and different linear and non-linear discriminant classifiers. They experimentally validated their proposed approach on the LIDC dataset. A fusion framework between PET and CT features has been proposed by Guo et al [10]. They applied SVM to train a vector of CT texture features and PET heterogeneity feature to improve the diagnosis and staging for lung cancer.

The existing methods for the classification of lung nodules have the following limitations: *(i)* some methods depend on the Hounsfield Unit (HU) values as the appearance descriptor without taking any spatial interaction into consideration; *(ii)* most of the reported accuracy is low compared to the clinically accepted threshold. *(iii)* some of the methods just depend on raw data and disregard the morphological information.

The proposed framework overcomes the previously mentioned limitations through the integration of a novel appearance feature using 7^{th}-order MGRF that take into account 3D spatial interaction between nodule's voxels, and geometrical features extracted from the segmented lung nodule with the deep autoencoder to achieve high classification accuracy.

2. METHODS

The proposed framework presents a new automated noninvasive clinical diagnostic system for the early detection of lung cancer by classification of the detected lung nodule as benign or malignant. It integrates appearance and geometrical information that are derived from a single computed tomography (CT) scan to significantly improve the accuracy, sensitivity, and specificity of early lung cancer diagnosis (Fig. 1). Two types of features are integrated together (appearance, and geometric features). The appearance feature is modeled using a Higher-Order Markov Gibbs Random Field (MGRF) that is used to relate the joint probability of the nodule appearance and the energy of repeated patterns in the 3D scans in order to describe the spatial inhomogenities in the lung nodule. The new higher 7^{th} -order MGRF model is developed in order to have the ability to model the existing spatial inhomogeneities for both small and large detected pulmonary nodules. Geometric features are extracted from the binary segmented nodules to describe the pulmonary nodule geometry. Details of the framework's main components are given below.

2.1. Appearance features using MGRF energy

Since the Hounsfield values' spatial distribution differs from benign nodules to malignant ones: the smoother homogeneity the nodule is, the more likely it is benign. Describing the visual appearance features using the MGRF model will distinguish between benign and malignant nodules showing high distinctive features (see Fig 2). To describe pulmonary nodules' texture appearance, Gibbs energy values are calculated using the 7^{th}-order MGRF model, to distinguish between benign and malignant nodules, because the Gibbs energy values shows the interaction between the voxels and their neighbors [11–14]. Let $\mathbb{Q} = \{0, \ldots, Q-1\}$; denote a finite set of signals (HU values) in the lung CT scan, $s : \mathbb{R}^3 \rightarrow \mathbb{Q}$, with signals $\mathbf{s} = [s(r) : r = (x, y, z) \in \mathbb{R}^3]$. The interaction graph, $\Gamma = (\mathbb{R}^3, \mathbb{E})$, quantifies the signal probabilistic dependencies in the images with nodes at voxels, $r \in \mathbb{R}^3$, that are connected with edges $(r, r') \in \mathbb{E} \subseteq \mathbb{R}^3 \times \mathbb{R}^3$. An MGRF of images is defined by a Gibbs probability distribution (GPD): $\boldsymbol{\Upsilon} = \left[\Upsilon(\mathbf{s}) : \mathbf{s} \in \mathbb{Q}^{|\mathbb{R}|}; \sum_{\mathbf{s} \in \mathbb{Q}^{|\mathbb{R}|}} \Upsilon(\mathbf{s}) = 1\right]$ factored over a set $\mathbb{C}$ of cliques in Γ supporting non-constant factors, logarithms of which are Gibbs potentials [15]. To make modeling more efficient at describing the visual appearance of different nodules in the lung CT scans, the 7^{th}-order MGRF models the voxel's partial ordinal interaction within a radius r rather than modeling the pairwise interaction as in the 2^{nd}-order MGRF.

Let a translation-invariant 7^{th}-order interaction structure on $\mathbb{R}$ be represented by A, $A \geq 1$, families, $\mathbb{C}_a$; $a = 1, \ldots, A$, of 7^{th}-order cliques, $\mathbf{c}_{a:r} \in \mathbb{C}_a$, of the same shape and size. Every clique is associated with a certain voxel (origin), $r = (x, y, z) \in \mathbb{R}^3$, supporting the same (7)-variate scalar potential function, $V_a : \mathbb{Q}^7 \rightarrow (-\infty, \infty)$.

The Gibbs probability distribution for this contrast/offset-, and translation-invariant MGRF is $\Upsilon_7(\mathbf{s}) = \frac{1}{Z}\phi(\mathbf{s}) \exp\left(-E_7(\mathbf{s})\right)$ where $E_{7:a}(\mathbf{s}) = \sum_{\mathbf{c}_{a:r} \in \mathbb{C}_a} V_{7:a}\left(g(r') : r' \in \mathbf{c}_{a:r}\right)$ and $E_7(\mathbf{s}) = \sum_{a=1}^{A} E_{7:a}(\mathbf{s})$ denote the Gibbs energy for each individual, and all the clique families, respectively; Z is a normalization factor, while $\phi(\mathbf{s})$ is a core distribution. The calculated Gibbs energy, $E_7(\mathbf{s})$, will be used to discriminate between benign and malignant tissues and gives an indication of malignancy. While a high potential of malignancy is indicated by lower energy, high potential to be benign is indicated by higher energy. To calculate $E_7(\mathbf{s})$, the Gibbs potentials for the 7^{th}-order model are calculated using the maximum likelihood estimates (MLE) by generalizing the analytical approximation in [16–20]:

$$V_{7:a}(\xi) = \frac{F_{7:a:\text{core}}(\xi) - F_{7:a}(\xi|\mathbf{s}^{\circ})}{F_{7:a:\text{core}}(\xi)\left(1 - F_{7:a:\text{core}}(\xi)\right)}; \qquad (1)$$

where $a = 1, \ldots, A$; $\xi \in \vartheta_7$, $\mathbf{s}^{\circ}$ denoted the training malignant nodule images; ξ denotes a numerical code of a particular 7^{th}-order relation between the 7 signals on the clique; ϑ_7 is a set of these codes for all 7^{th}-order signal co-occurrences; $F_{7:a}(\mathbf{s}^{\circ})$ is an empirical marginal probability of the relation ξ; $\xi \in \vartheta_7$, over the 7^{th}-order clique family $\mathbb{C}_{7:a}$ for $\mathbf{s}^{\circ}$, and $F_{7:a:\text{core}}(\xi)$ is the core probability distribution. The proposed 7^{th}-order MGRF appearance model is summarized in Algorithm 1.

2.2. Geometric features

As the lung nodules has different geometric characteristics based on whether it is malignant or benign , accounting for these differences as a discriminating features helps in the differentiation between different nodule types in the classification process. A set of seven geometric features will be extracted from the nodule's binary mask, (provided by radiologist). The following geometric features are calculated: *volume*, *surface area*, *convex volume*, *solidity*, *equivalent diameter*, *extent*, and the *principal axis length*. In order to calculate the *solidity*, a convex hull C is defined around the segmented nodule and the ratio between the volume of the voxels in C and the total volume of the segmented nodule is calcu-

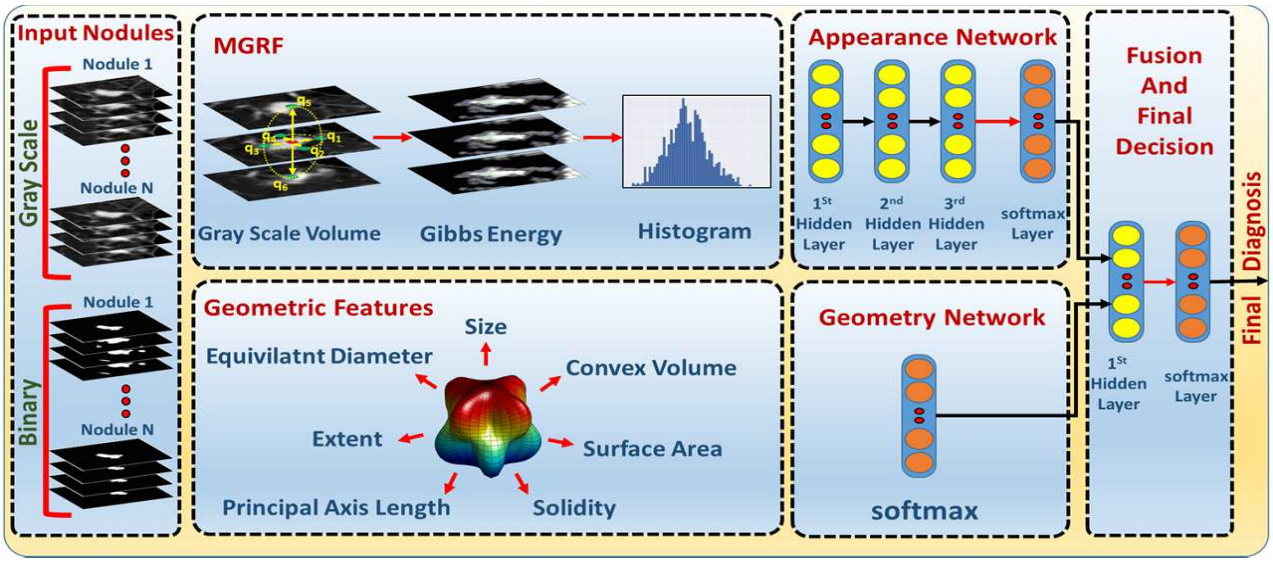

Fig. 1: Lung nodule classification framework.

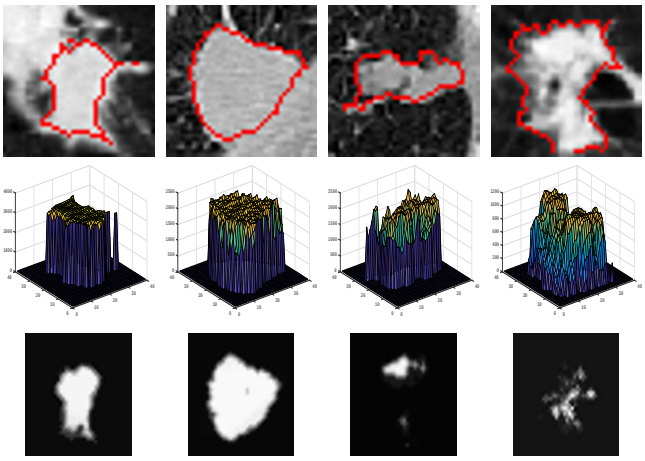

(a) (b) (c) (d)

Fig. 2: 2D axial projection for two benign *(a,b)* and two malignant *(c,d)* lung nodules *first-row*, along their 3D visualization of Hounsfield values *second-row*, and their calculated Gibbs energy *third-row*.

lated. Then, in order to calculate *extent*, the bounding box around the segmented nodule is used and the dimensions are named *dimx, dimy,* and *dimz* and the proportion of the volume of the voxels in the bounding cube to the volume of the voxels of the segmented nodule is calculated. *principal axis length* is defined as the largest dimension of the bounding cube *(max(dimx, dimy, dimz))*.

These features complement each other to come up with a final score for malignancy classification. To extract these features accurately without being dependent on scan accusation parameters such as pixel spacing and slice thickness, a volume of interest (VOI) of size $40 \times 40 \times 40\ mm^3$ that is centered around the center of each nodule is extracted and resampled to be an isotropic in the $x-$, $y-$, and $z-$ directions.

Algorithm 1 Learning the 7^{th}-order MGRF appearance model.

1. Given a training malignant nodules $\mathbf{g}^\circ$, find the empirical nodule ($l = 1$) and background ($l = 0$) probability distributions, $\mathbf{F}_{l:7:r}(\mathbf{g}^\circ) = [F_{l:7:r}(\beta|\mathbf{g}^\circ) : \beta \in \mathbb{B}]$ of the local binary pattern (LBP)-based descriptors for different clique sizes $r \in \{1, \ldots, r_{\max}\}$ where the top size $r_{\max} = 10$ in our experiments below.
2. Compute the empirical distributions $\mathbf{F}_{7:r:\text{core}} = [F_{7:r:\text{core}}(\beta) : \beta \in \mathbb{B}]$ of the same descriptors for the core independent random field (IRF) $\psi(\mathbf{g})$, e.g., for an image, sampled from the core.
3. Compute the approximate MLE of the potentials:

$$V_{l:7:r}(\beta) = \frac{F_{7:r:\text{core}}(\beta) - F_{l:7:r}(\beta|\mathbf{g}^\circ)}{F_{7:r:\text{core}}(\beta) \cdot (1 - F_{7:r:\text{core}}(\beta))}$$

4. Compute partial Gibbs energies of the descriptors for equal and all other clique-wise signals over the training image for the clique sizes $r = 1, 2, \ldots, 10$ to choose the size ρ_l, making both the energies the closest one to another.

2.3. Nodule classification using autoencoders

Our CADx system utilizes a feed-forward deep neural network to classify the pulmonary nodules whether malignant or benign, the implemented deep neural network comprises two-stage structure of stacked autoenocder (AE).

The first stage consists of two autoencoder-based classifiers, one classifier for the appearance, and one for the geometry, which are used to give an initial estimation for the probabilities of the classification, that are augmented together to be considered as the input for the second stage autoencoder to give the final estimation of the classification probabilities(see Fig. 1 for more details).

Autoencoder is employed in order to diminish the dimensionality of the input data (1000 histogram bins for the Gibbs energy image in the network of the appearance) with multi-layerd neural networks to get the most discriminating features by greedy unsu-

pervised pre-training.

After the AE layers,a softmax output layer is stacked in order to refine the classification by reducing the total loss for the training labeled input.

For each AE, let $W = \{W_j^e, W_i^d : j = 1, \ldots, s; i = 1, \ldots, n\}$ refer to a set of column vectors of weights for encoding, E, and decoding, D, layers, and let T denote vector transposition. The AE change the n-dimensional column vector $u = [u_1, , u_n]^T$ into an s-dimensional column vector $h = [h_1, , h_s]^T$ of hidden features such that $s < n$ by nonlinear uniform transformation of s weighted linear combinations of input as where $\sigma(.)$ is a sigmoid function with values from $[0, 1]$, $\sigma(t) = \frac{1}{1+e^{-t}}$,

Our classifier is constructed by stacking AE which consist of 3 hidden layers with softmax layer for the appearance network, the first hidden layer reduces the input vector to 500 level activators, while the second hidden layer continues the reduction to 300 level activators which are reduced to 100 after the third layer. The geometry network consists of the softmax layer only, as the input scale is not large enough to use AE with multiple hidden layers like the appearance network (only 9 geometric features) which compute the probability of being malignant or benign through the following equation:- $p(c; W_{o:c}) = \frac{e^{(W_{o:c}^T h^3)}}{e^{(\sum_1^c W_{o:c}^T h^3)}}$

Where $C = 1, 2$; denote the class number $W_{o:c}$: is the weighting vector for the softmax for class c; h^3: are the output features from the last hidden layer, (the third layer), of the AE. In the second stage, the output probability obtained from the softmax of the appearance, and geometry analysis networks, are fused together, and fed to another softmax layer to give the final classification probability.

3. EXPERIMENTAL RESULTS AND CONCLUSION

To train and test our proposed CADx system, the well-known Lung Image Database Consortium (LIDC) dataset is used. This Dataset consists of 1018 thoracic CT scans that has been collected from 1010 different patients from seven different academic centers. After removing the scans with slice thickness greater than $3mm$ and the scans with inconsistent slice spacing, a total of 888 CT scans became available for testing and evaluating our CADx system [21]. The LIDC CT scans are associated with an XML file to provide a radiological diagnosis for the lung lesions.All this diagnosis is provided by four radiologists in a two-phase image annotation process. In the first phase, each radiologist from the four radiologists independently reviewed all cases. The second phase is the final phase as each radiologist gives its final decision after checking the other three radiologists' decision.The radiologists divided the lesions into two groups nodules and non-nodules. We focused on the nodules $\geq 3mm$ as they have a malignancy score that vary from 1 as benign to 5 as malignant, and a well-defined contour annotated by the radiologists.

We trained our CAD system on a randomly selected sample of nodules. In order to be sure that the data is almost balanced, we used 413 benign and 314 malignant nodules. For each nodule the union of the four radiologists' mask is combined to obtain the final nodule mask that we will use in our experiments.A volume-of-interest (VOI) of size $40 \times 40 \times 40mm$ measured around the center of the nodule's combined mask is extracted for each nodule. The final diagnosis score of each nodule that we decided to work on is evaluated by calculating the average of the diagnosis scores for the four radiologists.

The system is evaluated by randomly dividing the dataset into two parts 70% for training and 30% for testing. The classification accuracy is described in terms of different measurement metrics, namely the specificity, sensitivity, precision, accuracy, and area under the curve (AUC). We reported the accuracy of the appearance model and the geometric model separately and for the complete fused system to highlight the effect of each model to the overall system (as shown in Table 1.).

Figure 3 shows the receiver operating characteristic (ROC) curve for each module and for the fused system as it is considered as a powerful tool to evaluate the discrimination of binary outcomes.The area under the ROC curve was 0.96, 0.87, and 0.97 for the appearance model, geometric model, and the fused system, respectively. In conclusion, this paper introduced a novel framework for the classification of lung nodules by modeling the nodules' appearance feature using a novel Higher-order MGRF in addition to geometric features. The classification results obtained from a set of 727 nodules collected from 467 patients confirm that the proposed framework holds the promise for the early detection of lung cancer. A quantitative comparison with recently developed diagnostic techniques highlights the advantages of the proposed framework over state-of -the-art ones. These promising results encourage us to model a new shape features and include it in the proposed framework in the future to reach the clinically accepted accuracy threshold, which is $\geq 95.00\%$.

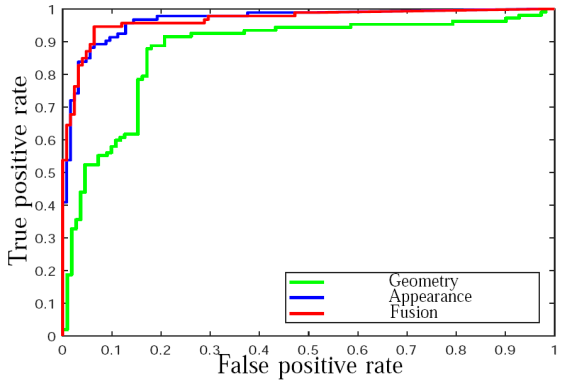

Fig. 3: ROC for different features and the combined ones.

Table 1: Classification results; in terms of Sensitivity, Specificity, Accuracy, Precision, and AUC; for different feature groups.

	Evaluation Metrics				
	Sens.	Spec.	Acc.	Prec.	AUC
Geometric	76.64	84.68	80.73	82.83	87.20
Appearance	93.55	87.20	89.91	84.47	96.66
Comb. Features	**92.22**	**92.19**	**92.20**	**89.25**	**96.70**

Table 2: Comparison between our proposed system and other four recent nodule classification techniques.

		Metric		
		Sensitivity	Specificity	Accuracy
Method	Kumar et al. [22]	83.35	–	75.01
	Hua et al. [23]	73.30	78.70	–
	Krewer et al. [24]	85.71	94.74	90.91
	Jiang et al. [25]	86.00	88.50	–
	Our system	**92.22**	**92.19**	**92.20**

4. REFERENCES

[1] American Cancer Society, "Cancer Facts and Figures," 2017.

[2] Karissa A Brazauskas, Jeanne B Ackman, and Benjamin Nelson, "Surveillance of actionable pulmonary nodules in children: The potential of thoracic mri," *Insights in Chest Diseases*, 2016.

[3] Lian-Ming Wu, Jian-Rong Xu, Jia Hua, Hai-Yan Gu, Jie Chen, EM Haacke, and Jiani Hu, "Can diffusion-weighted imaging be used as a reliable sequence in the detection of malignant pulmonary nodules and masses?," *Magnetic resonance imaging*, vol. 31, no. 2, pp. 235–246, 2013.

[4] Wenqing Sun, Bin Zheng, and Wei Qian, "Computer aided lung cancer diagnosis with deep learning algorithms," in *Medical Imaging 2016: Computer-Aided Diagnosis*. International Society for Optics and Photonics, 2016, vol. 9785, p. 97850Z.

[5] Wei Shen, Mu Zhou, Feng Yang, Caiyun Yang, and Jie Tian, "Multi-scale convolutional neural networks for lung nodule classification," in *International Conference on Information Processing in Medical Imaging*. Springer, 2015, pp. 588–599.

[6] Mizuho Nishio and Chihiro Nagashima, "Computer-aided diagnosis for lung cancer: usefulness of nodule heterogeneity," *Academic radiology*, vol. 24, no. 3, pp. 328–336, 2017.

[7] Ashis Kumar Dhara, Sudipta Mukhopadhyay, Anirvan Dutta, Mandeep Garg, and Niranjan Khandelwal, "A combination of shape and texture features for classification of pulmonary nodules in lung ct images," *Journal of digital imaging*, vol. 29, no. 4, pp. 466–475, 2016.

[8] QingZeng Song, Lei Zhao, XingKe Luo, and XueChen Dou, "Using deep learning for classification of lung nodules on computed tomography images," *Journal of healthcare engineering*, vol. 2017, 2017.

[9] Tizita Nesibu Shewaye and Alhayat Ali Mekonnen, "Benign-malignant lung nodule classification with geometric and appearance histogram features," *arXiv preprint arXiv:1605.08350*, 2016.

[10] Ning Guo, Ruoh-Fang Yen, Georges El Fakhri, and Quanzheng Li, "Svm based lung cancer diagnosis using multiple image features in pet/ct," in *Nuclear Science Symposium and Medical Imaging Conference (NSS/MIC), 2015 IEEE*. IEEE, 2015, pp. 1–4.

[11] Ni Liu, Ahmed Soliman, Georgy Gimelfarb, and Ayman El-Baz, "Segmenting kidney DCE-MRI using 1st-order shape and 5th-Order appearance priors," in *International Conference on Medical Image Computing and Computer-Assisted Intervention*. Springer, 2015, pp. 77–84.

[12] Ahmed Shaffie, Ahmed Soliman, Mohammed Ghazal, Fatma Taher, Neal Dunlap, Brian Wang, Adel Elmaghraby, Georgy Gimel'farb, and Ayman El-Baz, "A new framework for incorporating appearance and shape features of lung nodules for precise diagnosis of lung cancer," in *Image Processing (ICIP), 2017 IEEE International Conference on*. IEEE, 2017, pp. 1372–1376.

[13] Ayman El-Baz, Georgy Gimel'farb, Robert Falk, and Mohamed El-Ghar, "Appearance analysis for diagnosing malignant lung nodules," in *Biomedical Imaging: From Nano to Macro, 2010 IEEE International Symposium on*. IEEE, 2010, pp. 193–196.

[14] Aly A Farag, Ayman El-Baz, Georgy Gimelfarb, Robert Falk, Mohamed A El-Ghar, Tarek Eldiasty, and Salwa Elshazly, "Appearance models for robust segmentation of pulmonary nodules in 3d ldct chest images," in *International Conference on Medical Image Computing and Computer-Assisted Intervention*. Springer, 2006, pp. 662–670.

[15] Andrew Blake, Pushmeet Kohli, and Carsten Rother, *Markov random fields for vision and image processing*, MIT Press, 2011.

[16] G GimelFarb and AA Farag, "Texture analysis by accurate identification of simple markovian models," *Cybernetics and Systems Analysis*, vol. 41, no. 1, pp. 27–38, 2005.

[17] Ayman El-Baz, Georgy Gimelfarb, and Jasjit S Suri, *Stochastic modeling for medical image analysis*, CRC Press, 2015.

[18] Ayman El-Baz, Georgy Gimelfarb, Robert Falk, and M Abo El-Ghar, "3d mgrf-based appearance modeling for robust segmentation of pulmonary nodules in 3d ldct chest images," *Lung imaging and computer aided diagnosis*, vol. 3, pp. 51–63, 2011.

[19] Ayman El-Baz, Georgy Gimelfarb, Robert Falk, M Abo El-Ghar, and Jasjit Suri, "Appearance analysis for the early assessment of detected lung nodules," *Lung imaging and computer aided diagnosis*, vol. 17, pp. 395–404, 2011.

[20] Ayman El-Baz, Georgy Gimel'farb, Mohamed Abou El-Ghar, and Robert Falk, "Appearance-based diagnostic system for early assessment of malignant lung nodules," in *Image Processing (ICIP), 2012 19th IEEE International Conference on*. IEEE, 2012, pp. 533–536.

[21] Samuel G Armato, Geoffrey McLennan, Luc Bidaut, Michael F McNitt-Gray, Charles R Meyer, Anthony P Reeves, Binsheng Zhao, Denise R Aberle, Claudia I Henschke, Eric A Hoffman, et al., "The lung image database consortium (lidc) and image database resource initiative (idri): a completed reference database of lung nodules on ct scans," *Medical physics*, vol. 38, no. 2, pp. 915–931, 2011.

[22] Devinder Kumar, Alexander Wong, and David A Clausi, "Lung nodule classification using deep features in ct images," in *Computer and Robot Vision (CRV), 2015 12th Conference on*. IEEE, 2015, pp. 133–138.

[23] Kai-Lung Hua, Che-Hao Hsu, Shintami Chusnul Hidayati, Wen-Huang Cheng, and Yu-Jen Chen, "Computer-aided classification of lung nodules on computed tomography images via deep learning technique," *OncoTargets and therapy*, vol. 8, 2015.

[24] Henry Krewer, Benjamin Geiger, Lawrence O Hall, Dmitry B Goldgof, Yuhua Gu, Melvyn Tockman, and Robert J Gillies, "Effect of texture features in computer aided diagnosis of pulmonary nodules in low-dose computed tomography," in *Systems, man, and cybernetics (SMC), 2013 IEEE international conference on*. IEEE, 2013, pp. 3887–3891.

[25] Hongyang Jiang, He Ma, Wei Qian, Guohui Wei, Xinzhuo Zhao, and Mengdi Gao, "A novel pixel value space statistics map of the pulmonary nodule for classification in computerized tomography images," in *Engineering in Medicine and Biology Society (EMBC), 2017 39th Annual International Conference of the IEEE*. IEEE, 2017, pp. 556–559.